

# Damped Ly $\alpha$ absorbers at high redshift — large disks or galactic building blocks?

Martin G. Haehnelt<sup>1</sup>, Matthias Steinmetz<sup>1,2</sup>, Michael Rauch<sup>3,4</sup>

mhaehnelt@mpa-garching.mpg.de, msteinmetz@as.arizona.edu, mr@astro.caltech.edu

## ABSTRACT

We investigate the nature of the physical structures giving rise to damped Ly $\alpha$  absorption systems (DLAS) at high redshift. In particular, we examine the suggestion that rapidly rotating large disks are the only viable explanation for the characteristic observed asymmetric profiles of low ionization absorption lines. Using hydrodynamic simulations of galaxy formation in a cosmological context we demonstrate that irregular protogalactic clumps can reproduce the observed velocity width distribution and asymmetries of the absorption profiles equally well. The velocity broadening in the simulated clumps is due to a mixture of rotation, random motions, infall and merging. The observed velocity width correlates with the virial velocity of the dark matter halo of the forming protogalactic clump ( $\Delta v \approx 0.6 v_{\text{vir}}$  for the median values, with a large scatter of order a factor two between different lines-of-sight). The typical virial velocity of the halos required to give rise to the DLAS population is about  $100 \text{ km s}^{-1}$  and most standard hierarchical structure formation scenarios can easily account even for the largest observed velocity widths. We conclude that the evidence that DLAS at high redshift are related to large rapidly rotating disks with  $v_{\text{circ}} \gtrsim 200 \text{ km s}^{-1}$  is not compelling.

*Subject headings:* galaxies: kinematics and dynamics — galaxies: structure — intergalactic medium — quasars: absorption lines

---

<sup>1</sup>Max-Planck-Institut für Astrophysik, Postfach 1523, 85740 Garching, Germany

<sup>2</sup>Steward Observatory, University of Arizona, Tucson, AZ 85721, USA

<sup>3</sup>Astronomy Department, California Institute of Technology, Pasadena, CA 91125, USA

<sup>4</sup>Hubble Fellow

## 1. Introduction

Damped Ly $\alpha$  absorption systems (DLAS) have often been interpreted as large high-redshift progenitors of present-day spirals which have evolved little apart from forming stars (Wolfe 1988; Lanzetta et al. 1991; Wolfe 1995; Wolfe et al. 1995; Lanzetta, Wolfe & Turnshek 1995). A number of observational results have been quoted as being in support of this hypothesis (see section 6 below). Most recently, Prochaska & Wolfe (1997) have investigated a variety of idealised models for the spatial distribution and kinematics of the absorbing gas to test whether they could produce the absorption line profiles of low ionisation ionic species (LIS) associated with DLAS. Of those models they investigated, only the one in which the lines-of-sight (LOS) intersect rapidly rotating thick galactic disks can explain both the large velocity spreads (up to  $200\text{kms}^{-1}$ ) and the characteristic asymmetries of the observed LIS absorption profiles. In particular, they find that if they embed their disk model within a CDM structure formation scenario, the result is inconsistent with the observed velocity widths. In this paper we demonstrate that the inconsistency with galaxy formation models within hierarchical cosmogonies (e.g. Kauffmann 1996) disappears if the gas is modeled with a more realistic spatial distribution and kinematic structure.

For this purpose we use numerical simulations of galaxy formation in a CDM cosmogony including gas dynamics and realistic initial conditions. These exhibit a complex relationship between high column density absorption features and the underlying dark matter distribution (Katz et al. 1996; Haehnelt, Steinmetz & Rauch 1996, paper I; Rauch, Haehnelt & Steinmetz 1997, paper II; Gardner et al. 1997a/b). Agglomerations of neutral hydrogen with central column densities larger than  $10^{20}\text{cm}^{-2}$  and with the masses of dwarf galaxies do occur commonly in these simulations. These objects form by gravitational collapse in CDM potential wells. Subsequent cooling produces an optically thick, mostly neutral phase in the inner ten to twenty kpc. We have already demonstrated that the large number of these objects and their clustering and merging into larger units can explain many observed features of metal absorption systems, for example the ionization and thermal state of the gas, and the observed multi-component structure of the absorption line profiles (paper I&II). In these models the high rate of incidence of damped Ly $\alpha$  systems is a result of the high abundance of protogalactic clumps (PGC) which are the progenitors of large present-day galaxies. This must be contrasted with the popular picture of DLAS where a population of very large disks evolves without merging to form present-day spirals.

Prochaska & Wolfe (1997) have highlighted two crucial questions which a hierarchical structure formation model must be able to address satisfactorily:

- (1) How do the observed asymmetries of the absorption line complexes arise?
- (2) Can absorption by groups of PGCs in a hierarchical universe reproduce the observed velocity width distribution?

Below we will investigate the velocity width and shape of LIS absorption profiles using

artificial spectra for lines-of-sight through numerically simulated regions of ongoing galaxy formation. We then examine the underlying physical conditions responsible for the kinematic structure of these systems. We further investigate the connection between the velocity width of the absorption systems and the depth of the forming potential well and assess the problem of accommodating the observed velocity width within standard hierarchical cosmogonies. Finally we discuss our results and some other, observational clues to the nature of DLAS, and draw conclusions.

## 2. Numerical simulations of damped Ly $\alpha$ systems

### 2.1. The hydrodynamical simulations

Spatial regions of the universe selected to contain one or a few normal galaxies at redshift zero are simulated with the hydrodynamic GRAPE-SPH code (Steinmetz 1996) in the framework of a standard CDM cosmogony ( $\sigma_8 = 0.67$ ,  $H_0 = 50 \text{ km s}^{-1} \text{ Mpc}^{-1}$ ,  $\Omega_b = 0.05$ ). Temperature, density and peculiar velocity arrays along LOS through the simulated boxes are used to produce artificial absorption spectra. For a detailed description of the properties of the simulations and the resulting absorption features see Steinmetz (1996), Navarro & Steinmetz (1997), and papers I&II. The strategy of simulating small regions of ongoing galaxy formation preselected from a large dark matter simulation allows us to achieve a spatial resolution of 1 kpc and a mass resolution of  $5 \times 10^6 M_\odot$  (in gas). This high resolution — about a factor ten higher than that in most other cosmological hydro-simulations — is crucial to resolve the rich substructure within the damped region induced by the frequent merging of protogalactic clumps in hierarchical structure formation scenarios. Despite this, the resolution is still not sufficient to account for a possible clumping on sub-kpc scales due to thermal instabilities (Mo 1994; Mo & Miralda-Escudé 1996). Furthermore energy and momentum feedback due to star formation are not included. Both effects are likely to produce additional substructure in physical as well as in velocity space.

### 2.2. The region of neutral hydrogen — self-shielding

To study the kinematic structure of damped systems we extend our previous work to LOS passing through regions of collapsed dark matter halos with integrated HI column densities exceeding  $2 \times 10^{20} \text{ cm}^{-2}$ . The main problem which then arises is the treatment of the self-shielding of the dense gas against radiation beyond the Lyman edge. With the current generation of computers it is not yet possible to run cosmological hydro-simulations which solve the full radiative transfer equations. We therefore have adopted a simple scheme to mimic the effect of self-shielding which is motivated by the tight correlation between column density and density predicted by the numerical simulations (Miralda-Escudé et al 1996; paper II). A HI column density of  $10^{17} \text{ cm}^{-2}$ , above which self-shielding becomes important, occurs for LOS with an absorption-weighted density

of about  $10^{-3} \text{ cm}^{-3}$  to  $10^{-2} \text{ cm}^{-3}$ . This is easy to understand by looking at the photoionization equilibrium equation for a highly ionized optically thin homogeneous slab of hydrogen. The column density of neutral hydrogen then scales as  $N_{\text{HI}} \propto n_{\text{H}}^2 D J_{912}^{-1}$ , where  $D$  is the thickness of the slab and  $J_{912}$  is the flux of the UV background at the Lyman edge. The hydrogen density at the onset of self-shielding in the central plane can be written as,

$$n_{\text{shield}} \sim 3 \times 10^{-3} \left( \frac{D}{10 \text{ kpc}} \right)^{-0.5} \left( \frac{J_{912}}{0.3 \times 10^{21} \text{ erg cm}^{-2} \text{ sec}^{-1} \text{ Hz}^{-1} \text{ sr}^{-1}} \right)^{0.5} \text{ cm}^{-3}, \quad (1)$$

where the spectral shape proposed by Haardt & Madau (1996) was used to transform the flux at the Lyman edge  $J_{912}$  into a photoionization rate. The geometry of collapsed regions in the numerical simulations is certainly more complicated than that of a slab, but  $D = 10 \text{ kpc}$  is a typical scale. To be on the safe side we assumed that all the gas above a density threshold of  $10^{-2} \text{ cm}^{-2}$  is self-shielded. This probably underestimates the size of the self-shielding region.

### 2.3. Profiles of low ionization ionic species

In observed DLAS hydrogen is predominantly neutral due to the self-shielding of the gas while the other atomic species attain low ionization states (Viegas 1995). Optically thin transitions of LIS like SiII AlII, FeII and NiII are therefore generally considered as suitable tracers of the kinematic and density structure of the neutral gas (Wolfe 1995). We have chosen the SiII 1808 absorption feature for our investigation. Silicon was assumed to be predominantly in the first ionization state within the self-shielding region,

$$\frac{[\text{SiII}]}{[\text{Si}]} = 1, \quad n_{\text{H}} > 10^{-2} \text{ cm}^{-3},$$

$$\frac{[\text{SiII}]}{[\text{Si}]} = 0, \quad \text{otherwise.}$$

A homogeneous silicon abundance of  $[\text{Si}/\text{H}] = -1$  was assumed for the self-shielding region. Artificial spectra were made to resemble typical Keck data obtainable within a few hours from a 16-17th magnitude QSO (S/N= 50 per  $0.043 \text{ \AA}$  pixel, FWHM = 8km/s). To make contact with our previous work we will also show the corresponding CIV absorption line profiles. For these a homogeneous carbon abundance of  $[\text{C}/\text{H}] = -1.5$  was assumed. The CIV fraction was calculated using the photoionization code CLOUDY (Ferland 1993) as described in papers I&II.

### 2.4. A gallery of simulated damped Ly $\alpha$ absorbers

Figs 1-5 present some typical examples of simulated damped Ly $\alpha$  absorption systems. The *bottom left* panel shows the absorption spectrum for the SiII 1808 and CIV 1548 transitions, the

*top left* and *bottom right* show the total hydrogen density and peculiar velocity along the LOS, while the *top right* panel shows density and velocity fields in a thin slice containing the LOS. The coordinates are proper distance, and the projection is such that the LOS along which the absorption spectrum is determined lies along the z-axis. The wavelength axis of the spectra is in  $\text{km s}^{-1}$ . Velocities are relative to the center-of-mass velocity of a sphere with 30 kpc radius. The assumed density threshold for self-shielding is indicated by the dashed line in the density profile and by the thick contour in the slice of the density field.

Fig. 1 shows a typical example of two merging PGCs. The density profile along the line of sight has two peaks within the self-shielding region. On larger scales the gas is flowing in from the left and the right, but in the self-shielded region the flow is rather quiescent with a velocity gradient of only about  $30 \text{ km s}^{-1}$ . This results in a double-peaked SiIII 1808 absorption profile with about  $30 \text{ km s}^{-1}$  velocity difference between the peaks.

Fig. 2 shows another example of merging PGCs. This time the density profile along the line of sight has three rather marginal peaks within the self-shielding region. The velocity profile is smooth but shows large gradients due to an eddy-like motion in the shock produced by the infalling clump. The corresponding SiIII 1808 absorption profile is complex and extends over  $200 \text{ km s}^{-1}$ , showing a prominent leading edge. The hump in the velocity profile at 5kpc and the three density peaks show all up as individual absorption features.

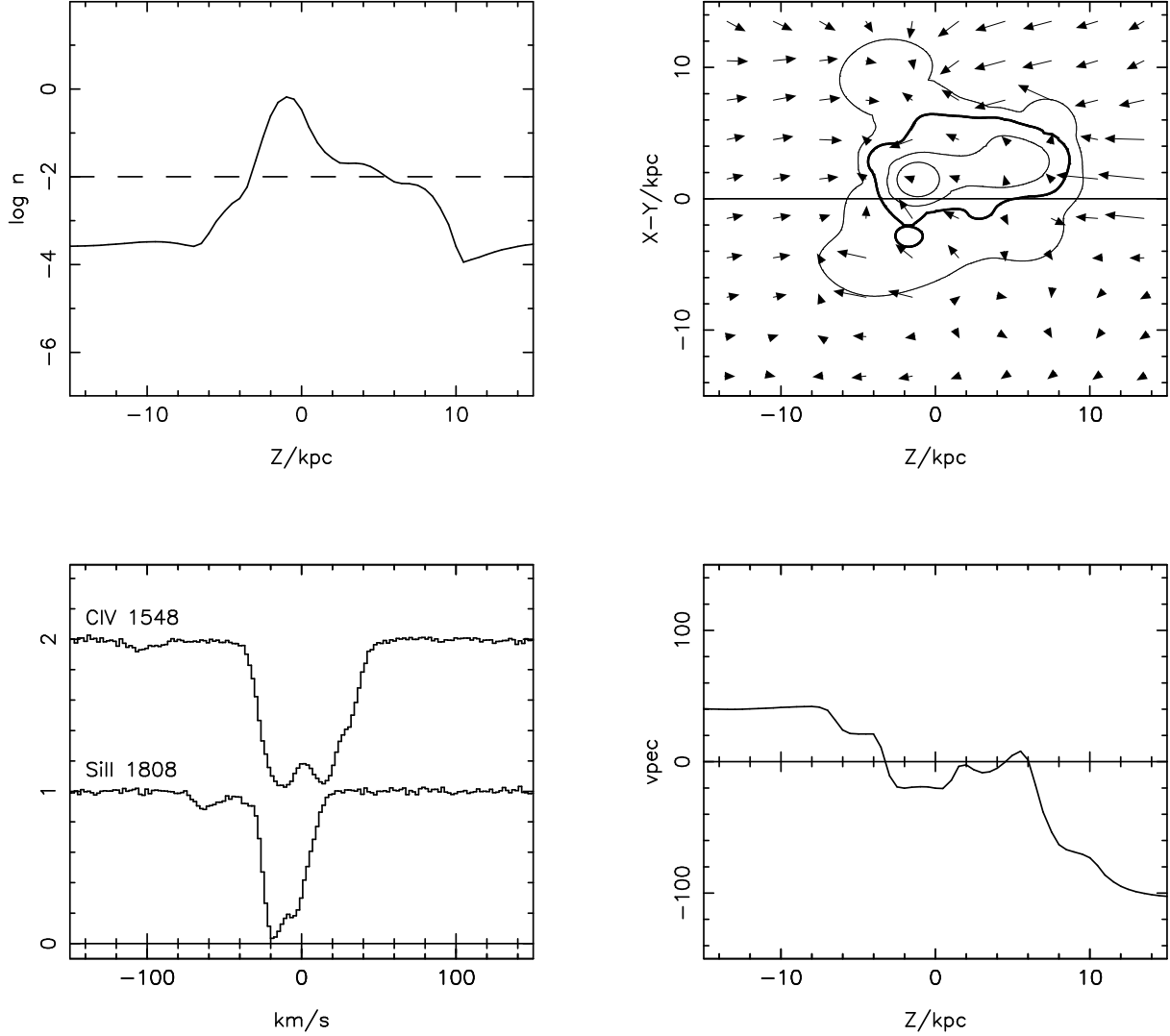


Fig. 1.— Simulated damped  $\text{Ly}\alpha$  absorber at  $z = 2.1$  with  $\log N_{\text{HI}} = 21.2$  arising from gas in a merging protogalactic clump with  $v_{\text{vir}} = 70 \text{ km s}^{-1}$ . *Bottom left:* Absorption spectrum for the SiII 1808 and CIV 1548. transitions. *Top left:* Total hydrogen density along the LOS. *Bottom right:* Peculiar velocity along the LOS. *Top right:* Density and velocity field in a thin slice containing the LOS (straight solid line). The density contours have a spacing of 1 dex and the thick contour marks  $\log n = -2$ . Velocities are relative to the center-of-mass velocity of a sphere with 30 kpc radius. The normalization of the velocity arrows is such that the length of the longest arrow equals the spacing between arrows. For absolute velocity values see the bottom right panel.

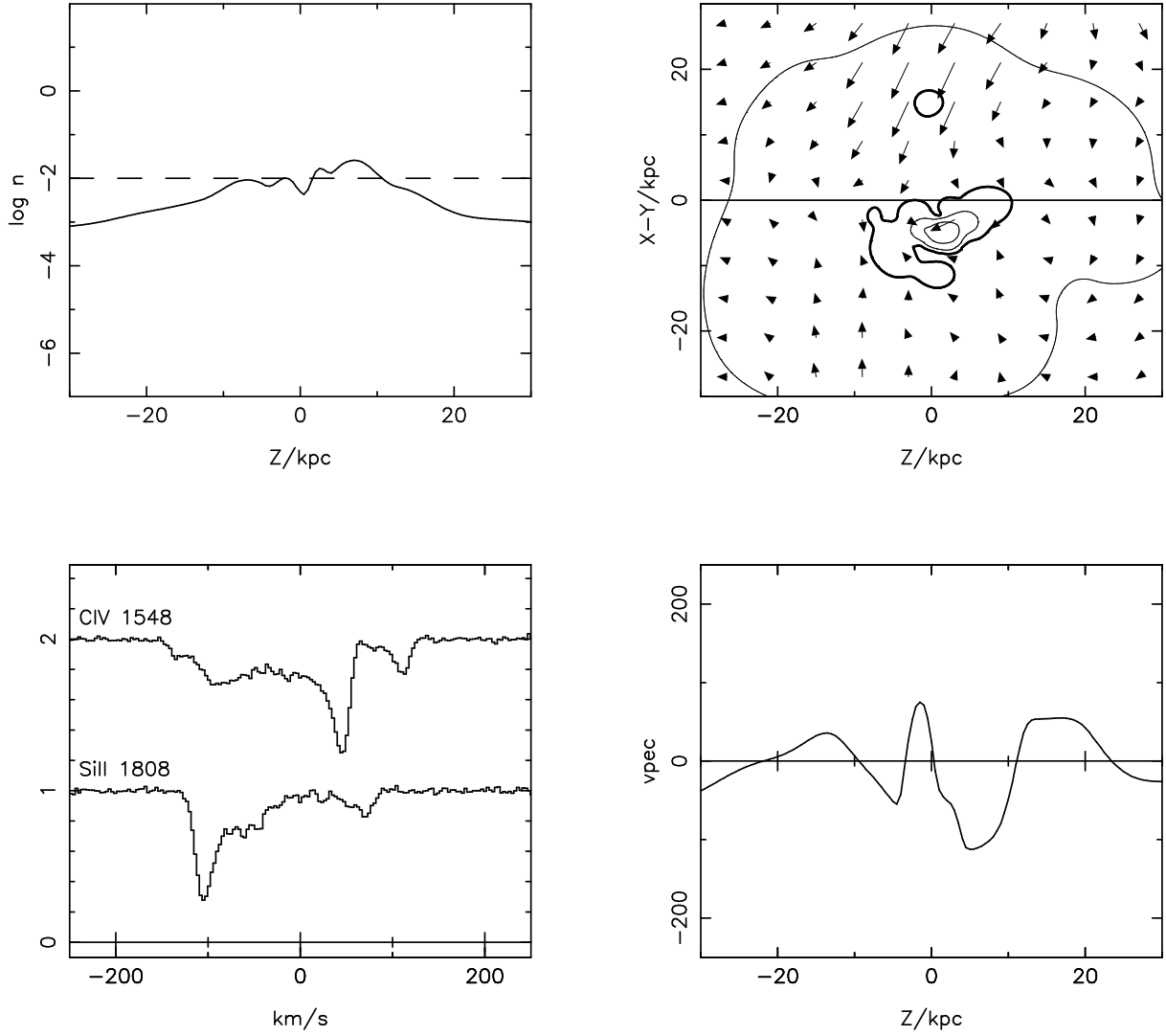


Fig. 2.— Simulated damped  $\text{Ly}\alpha$  absorber at  $z = 3.1$  with  $\log N_{\text{HI}} = 20.6$  arising from gas in a merging protogalactic clump with  $v_{\text{vir}} = 65 \text{ km s}^{-1}$ .

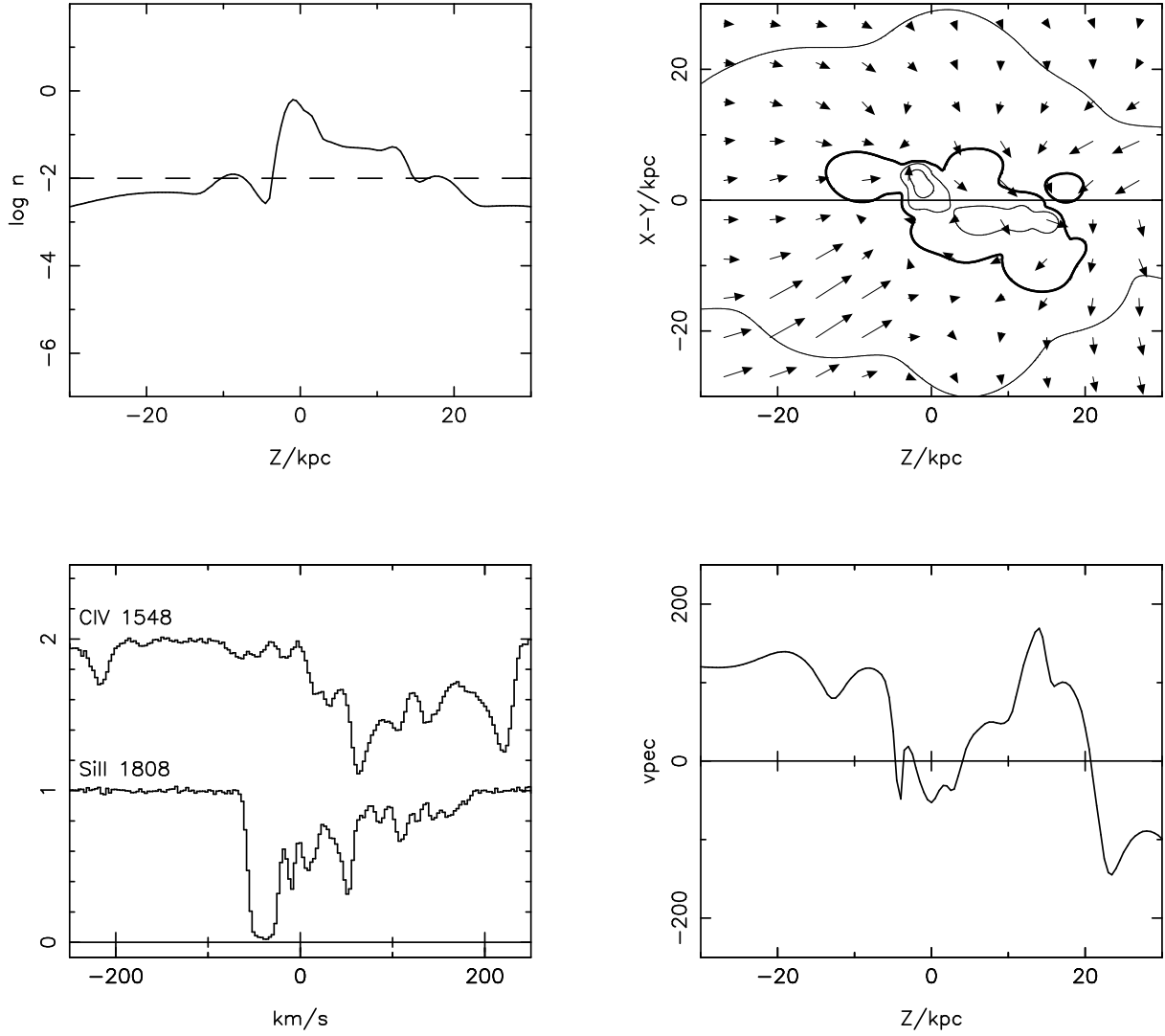


Fig. 3.— Simulated damped Ly $\alpha$  absorber at  $z = 3.1$  with  $\log N_{\text{HI}} = 21.7$  arising from gas in a merging protogalactic clump with  $v_{\text{vir}} = 200 \text{ km s}^{-1}$ .



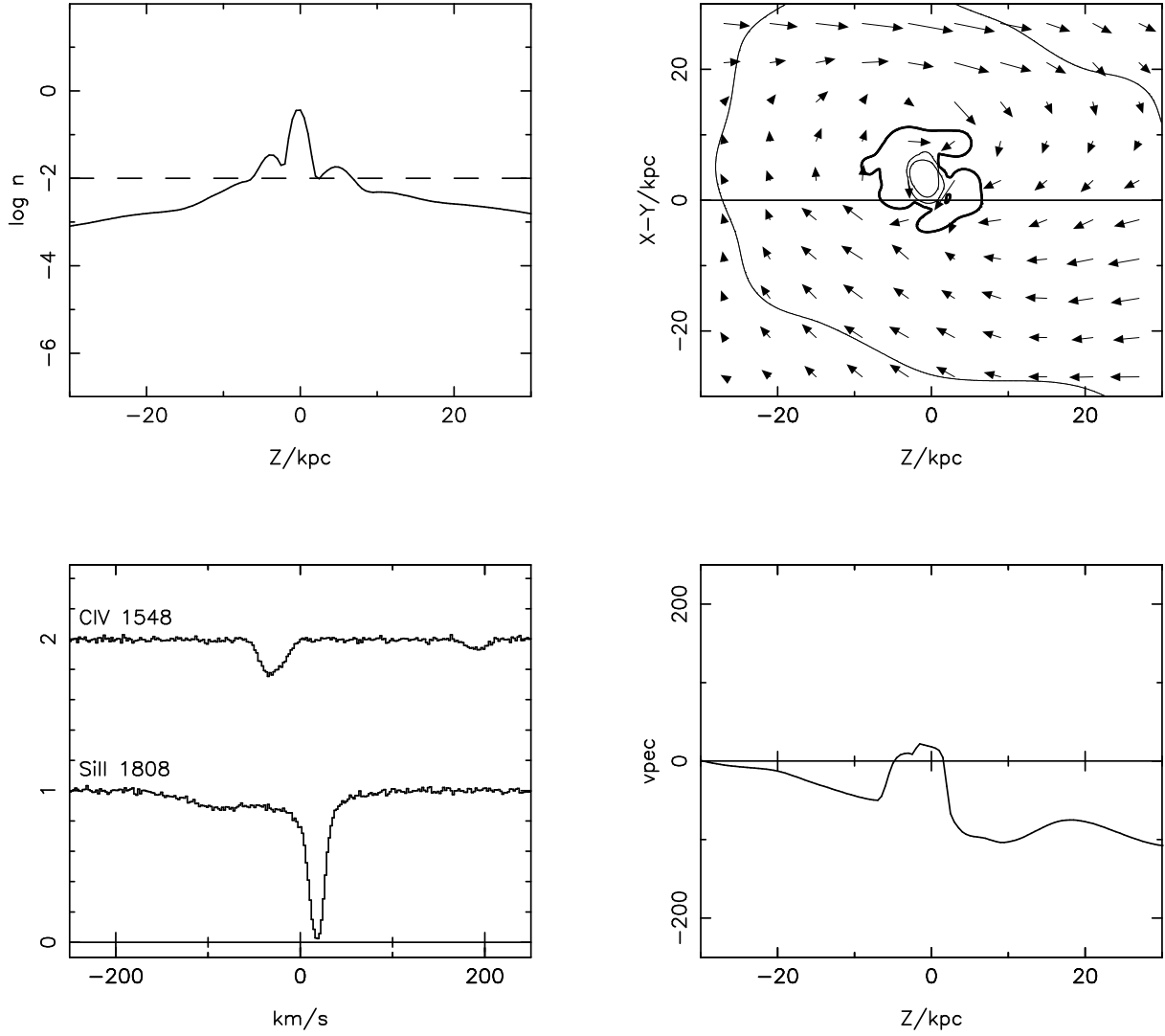


Fig. 4.— Simulated damped  $\text{Ly}\alpha$  absorber at  $z = 2.1$  with  $\log N_{\text{HI}} = 21.3$  arising from gas in a “rotating” protogalactic clump with  $v_{\text{vir}} = 180 \text{ km s}^{-1}$ .

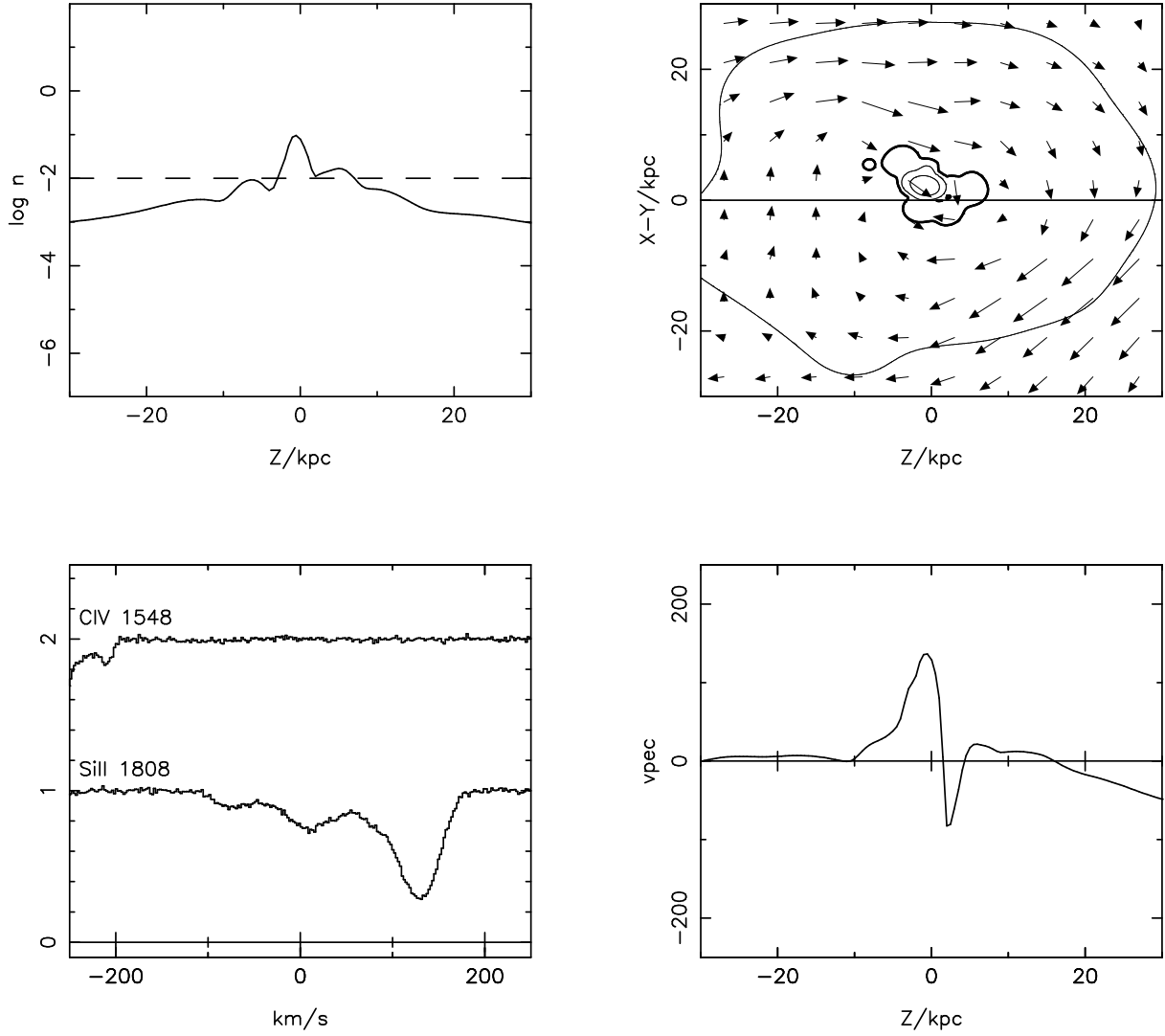


Fig. 5.— Simulated damped Ly $\alpha$  absorber at  $z = 2.1$  with  $\log N_{\text{HI}} = 20.8$  arising from gas in a “rotating” protogalactic clump with  $v_{\text{vir}} = 180 \text{ km s}^{-1}$ .

Fig. 3 shows a similar third example of merging PGCs. The peculiar velocity profile shows the same large gradients but is much more chaotic than that in Fig. 2. The peaks of the density profiles and the features of the velocity profile in the self-shielding region can again be identified in the SiII1808 absorption profile which also shows a prominent leading edge. One should note here the strong difference between the SiII 1808 profile and the CIV 1548 profile. The latter arises from absorption by the spatially separated warm gas surrounding the self-shielding region.

Fig. 4 and 5 show two of the rather rare cases where there is a large rotational component in the motion of the gas. For these “rotating” PGCs we generally find rather smooth density and velocity profiles in the self-shielding region. In most cases these result in single-peaked SiII 1808 absorption profiles with mild asymmetries or extended wings to one side as in Fig. 4. The latter are often difficult to detect unless the main peak is already saturated. The best example of a leading edge profile produced by rotation which we could find is shown in Fig. 5.

## 2.5. Orientation effects

As discussed above, the detailed structure of the absorption profile of the LIS regions depends strongly on the substructure in physical and velocity space. This makes the absorption profiles very sensitive to the orientation of the LOS. In order to demonstrate this we plot in Fig. 6 ten different randomly oriented LOS, each giving rise to damped Ly $\alpha$  absorption, in the vicinity of the PGC shown in Fig. 1. The nature of the absorption profiles varies from a single symmetric peak to double and multiple peaks. The rapid changes in the details of the velocity profile along the LOS are due to the rather chaotic velocity field of the merging PGC, and are the main reason for the dramatic changes in the LIS absorption profile. It is also clearly seen that the absorption profile of the higher ionization ion CIV varies independently of SiII. This is due to the fact that CIV arises mainly from the warmer gas outside the self-shielding region.

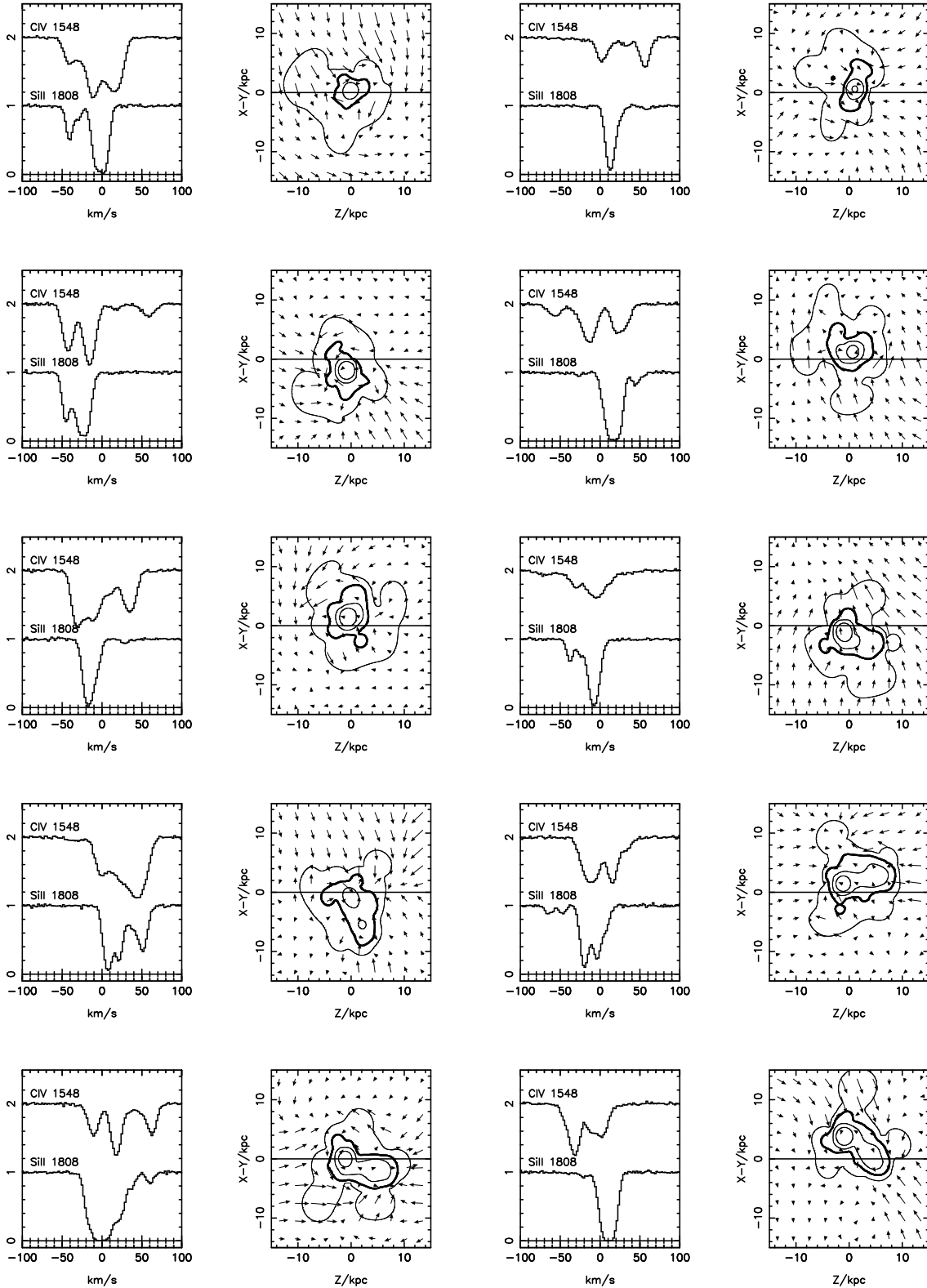


Fig. 6.— Ten random LOS producing damped Ly $\alpha$  in the vicinity of the merging protogalactic clump shown in Fig. 1. Plotted are absorption spectra and corresponding density/velocity fields as in the top right and bottom left panels of Fig. 1.

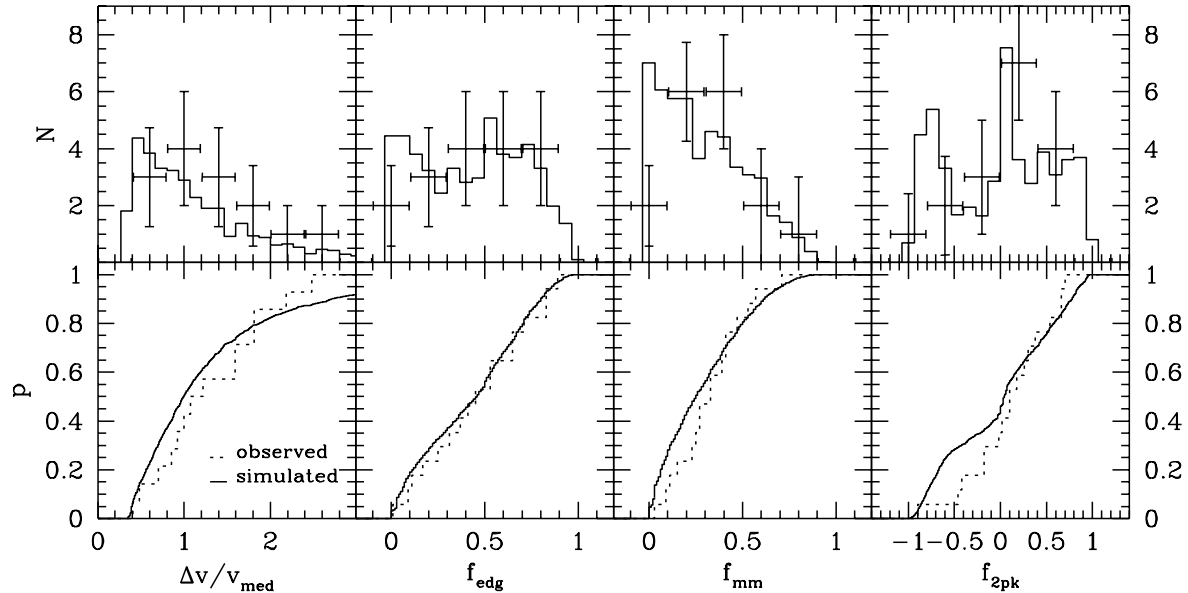


Fig. 7.— Velocity width distribution and shape parameter — From left to right: velocity width (relative to the median value), edge-leading index, mean-median index and 2-peak index. The top panels show the differential distribution in absolute numbers (model curves normalized to the observed number of systems); the bottom panels show the cumulative probability distribution. The data is taken from Prochaska & Wolfe (1997).

### 3. Distribution of velocity widths and shapes — Observed *vs* simulated

Prochaska & Wolfe (1997) have introduced four parameter to characterize LIS absorption profiles. In order to facilitate comparison with their observed sample of DLAS (a sample of 17 DLAS obtained by Sargent et al. with the Keck HIRES instrument) we have applied their selection criteria and characterized the simulated LIS profiles in exactly the same manner. The SiII 1808 absorption profiles were transformed into an apparent optical depth profile which was then smoothed over a range of 9 pixels. The first parameter — the velocity width  $\Delta v$  of the LIS region — is defined as the velocity interval which contributes the central 90 percent to the optical depth weighted velocity integral,

$$\tau_{\text{tot}} = \int \tau dv. \quad (2)$$

The mean velocity  $v_{\text{mean}}$  is defined as the midpoint of the velocity width interval (setting  $v = 0$  at the left edge) while the median velocity  $v_{\text{med}}$  bisects the integral in equation (2) performed over the velocity width interval. The three shape parameters designed to detect asymmetries in the

absorption complexes are defined as follows,

$$f_{\text{edg}} = \frac{|v_{\text{pk}} - v_{\text{mean}}|}{(\Delta v/2)}, \quad (3)$$

$$f_{\text{mm}} = \frac{|v_{\text{median}} - v_{\text{mean}}|}{(\Delta v/2)}, \quad (4)$$

$$f_{2\text{pk}} = \pm \frac{|v_{2\text{pk}} - v_{\text{mean}}|}{(\Delta v/2)}, \quad (5)$$

where  $v_{\text{pk}}$  and  $v_{2\text{pk}}$  are the velocity of the highest and second highest significant peak in the smoothed apparent optical depth profile. For the 2-peak test the plus (minus) sign holds if the velocity of the second peak falls (falls not) between the velocity of the first peak and the mean velocity. In the case of single peaks  $f_{2\text{pk}}$  is set equal to  $f_{\text{edg}}$ . To avoid saturation effects and to ensure sufficient signal-to-noise only absorption profiles with

$$0.1 \leq \frac{I_{\text{pk}}}{I_0} \leq 0.6 \quad (6)$$

were considered, where  $I_{\text{pk}}$  and  $I_0$  are the intensity of the strongest peak and the continuum respectively.

A sample of 640 simulated damped Ly $\alpha$  absorption systems with column densities above  $2 \times 10^{20} \text{ cm}^{-2}$  and satisfying the criterion in equation (6) was assembled by choosing random LOS in the vicinity of 40 protogalactic clumps identified with a friends-of-friends group-finder. For the discussion of velocity widths a minimum threshold of  $\Delta v > 30 \text{ kms}^{-1}$  was imposed on both the observed and simulated velocity widths to avoid incompleteness effects. The redshift of the simulated DLAS is  $z = 2.1$ , the median redshift of the observed sample.

Fig. 7 summarizes the comparison between the observed and simulated samples. The top panels show the differential distributions of the velocity width, the edge-leading, the mean-median, and the 2-peak parameter. The observed sample is still small and we therefore had to use rather large bins for the observed data. The absolute numbers of the observed sample are plotted while the simulated sample is normalized accordingly. The error bars indicate the Poisson errors and

Table 1. KS tests observed vs simulated.

KS Probabilities for P&W Tests			
$P_{\Delta v}$	$P_{\text{edg}}$	$P_{\text{mm}}$	$P_{2\text{pk}}$
0.69	0.98	0.23	0.28

the width of the bin respectively. The velocity width is plotted relative to the median value of the observed sample and relative to the median value of subsamples of 16 LOS around each PGC in the simulated sample. This allows us to test the relative velocity distribution independent of the cosmological model chosen. We come back to the absolute velocity width of the LIS region in section 5. The bottom panels show the corresponding cumulative distribution. The agreement between observed and simulated spectra is within the expected statistical errors. The KS test values for the cumulative distribution are given in Table 1. For none of the parameters is the KS test probability smaller than 20%. We would, however, like to caution against using KS tests to discriminate between different models. Small KS probabilities can be very misleading if a very special representation of a general class of models is chosen. We have e.g. varied our density threshold for the self-shielding region, the redshift of the sample and the metallicity of the gas and found significant changes in the distribution of the parameter. In some cases they further improved the agreement, and in some cases they led to KS probabilities as small as a tenth of a percent for one or two of the parameters. We believe that a significantly larger sample and a careful assessment of the selection effects are necessary in order to draw strong conclusions from the detailed distributions of the shape parameters introduced by Prochaska & Wolfe.

#### 4. Physical conditions giving rise to damped Lyman $\alpha$ systems

In the previous section we have shown that LOS passing the vicinity of PGCs can give rise to DLAS with LIS absorption profiles which reproduce the characteristic velocity width distribution and asymmetries of observed DLAS. It remains to be seen which underlying physical conditions are giving rise to these features. In hierarchical structure formation scenarios the “progenitor” of a present-day galaxy consists of several PGCs often moving along filamentary structures to merge into larger objects. We found the turbulent gas flows and inhomogeneous density structures related to the merging of two or more clumps to be the main reason for the occurrence of multiple LIS absorption systems with large velocity widths. Rotational motions of the gas play only a minor role for these absorption profiles, as does the velocity broadening due to the Hubble expansion between aligned clumps which is important for higher ionization species like CIV (see papers I&II). The latter is easily understandable given the small cross section of the LIS region.

##### 4.1. Properties of the absorbing protogalactic clumps

We have systematically investigated the physical properties of our sample of 40 PGCs in order to understand what kind of motions are reflected in the LIS line profiles and how their velocity width is related to the depth of the potential wells in which they are embedded. For this purpose we determined the following quantities for the absorbers: total velocity dispersion of the large scale motions of the gas in the self-shielding region, velocity dispersion due to radial motions of the gas, overall rotational velocity of the gas and virial velocity of the dark matter halo. The virial

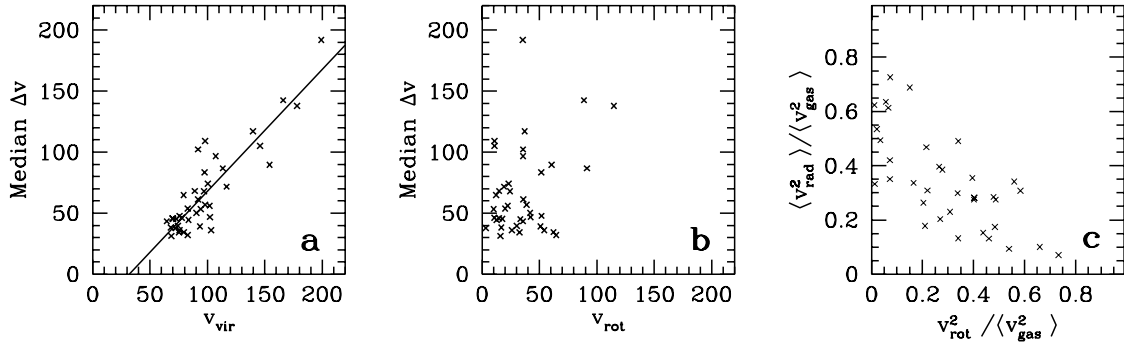


Fig. 8.—

- a) Median velocity width of the LIS region for random LOS around 40 protogalactic clumps (Median of 16 LOS per PGC) *vs* virial velocity of the associated DM halo.
- b) Median velocity width *vs* mean rotational velocity of the gas.
- c) Relative contributions of rotation and radial infall to the motion of the gas.

velocity is defined as  $v_{\text{vir}} = \sqrt{GM/r}$  in a sphere overdense by a factor 200 compared to the mean cosmic density. One should note here that the DM halo(s) are not necessarily virialized during the merger of two PGCs.

In Fig. 8a the median value of the velocity width for 16 randomly orientated LOS around each PGC is plotted *vs* the virial velocity of the DM halo. There is a strong correlation indicating that the velocity width reflects the depth of the potential reasonably well even though there is considerable scatter. The velocity width of the LIS absorption region is typically 60 percent of the virial velocity of the DM halo. The solid line shows the least-square fit.

Fig. 8b shows the relation between rotational velocity and velocity width. There seems to be no correlation. The rotational velocity is generally too small to account for the observed LIS velocity width. In Fig. 8c the relative contribution of radial motions and rotation to the total velocity dispersion of the gas is shown. The contributions of rotation and radial motions (mainly infall and merging) range between 0 and 70 percent. As expected these are anti-correlated. The contribution of additional random motions is generally between 30 and 70 percent.

#### 4.2. How do asymmetric and leading edge profiles arise?

The main motivation for interpreting observed absorption profiles as a signature of rotation are their leading edges, *i.e.*, the strongest absorption feature often occurs at one of the edges of the profile. As demonstrated by Prochaska & Wolfe (1997) such profiles occur naturally in a thick disk model with an exponential density and an isothermal velocity profile. Fig. 5 shows such an example. There is, however, an equally simple and plausible explanation for such leading edges in a scenario of merging protogalactic clumps. In the case of two merging clumps the strongest absorption feature will generally be caused by the high density central region of the clump which



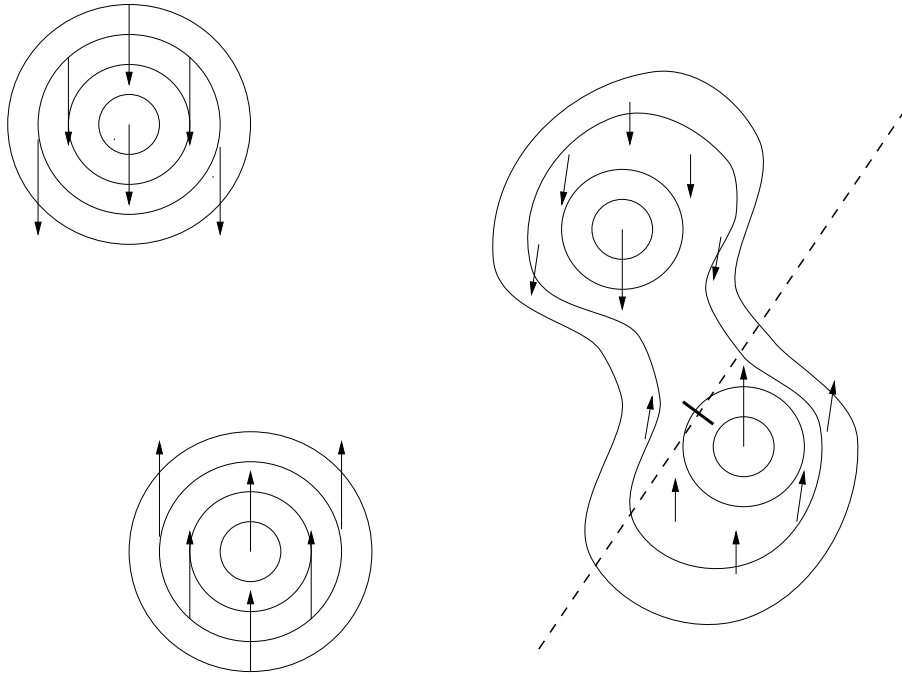


Fig. 9.— A schematic view how leading edges arise from merging protogalactic clumps. The dashed line represents a random line-of-sight with the expected position of the strongest absorption feature marked.

is closest to the LOS. The dense regions of merging PGC will move faster than their surroundings because of the smaller deceleration by the (density-dependent) ram pressure. The strongest absorption feature then occurs naturally at the edge of the absorption profile. Smaller features are produced by density fluctuations in stripped material behind or by shocked material in front of the dense region. This situation is illustrated schematically in Fig. 9. Except in the rare case where the LOS passes both dense regions symmetrically this is an intrinsically asymmetric configuration in velocity space. This is the principal reason for the asymmetric LIS absorption profiles in our models. We caution, however, against over-interpretation of leading edge profiles. One should keep in mind that in the case of three randomly ordered components of varying strength the probability that the strongest component is at one edge is  $2/3$  and in the case of four components it is still  $1/2$ .

## 5. Absolute velocity widths and cosmological models.

In section 3 we have shown that the width distribution of the simulated LIS profiles relative to its median value is consistent with that observed, and in section 4.1 we demonstrated that the width of the profiles is correlated with the the virial velocity of the associated DM halo. Fig. 10a shows the complete velocity width distribution of the 640 DLAS in our sample. The median value

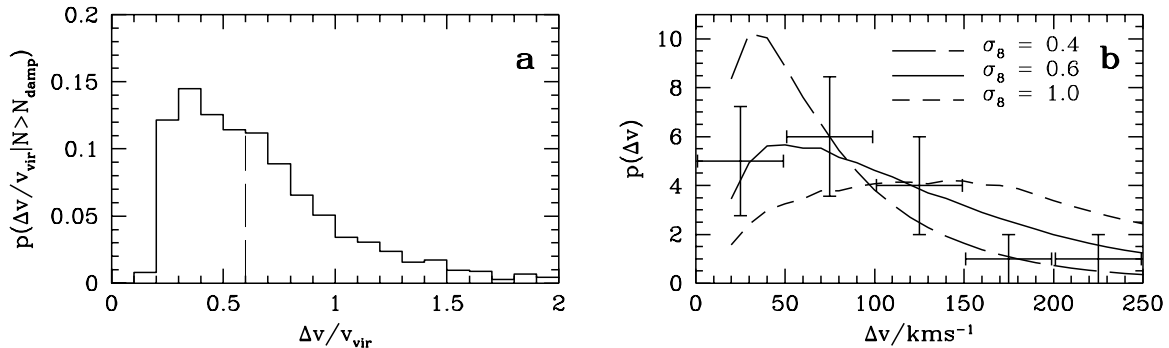


Fig. 10.—

a) Probability distribution of the velocity width scatter relative to the virial velocity of the associated DM halo of the PGC giving rise to the damped absorption system for 640 random LOS. The dashed line indicates the median value of 0.6.

b) Probability distribution of absolute velocity widths at  $z = 2.1$  for CDM models with varying  $\sigma_8$  as indicated on the plot. Crosses are the observed values from Prochaska & Wolfe (1997).

is about 60 percent of the virial velocity of the associated DM halo,

$$\text{median}(\Delta v) \approx 0.6 \times v_{\text{vir}}. \quad (7)$$

This value depends somewhat on the assumed density threshold for self-shielding, the assumed metallicity, the selection criterion of the PGC and the redshift of the sample. Varying these parameter we found the ratio of velocity width to virial velocity to vary between 0.5 and 0.75. One should note here that the virial velocity which we infer from a given velocity width is a factor 1.5 to 2.5 times smaller than in the rotating disk model.

It is difficult to assure that the sample of PGCs picked from our numerical simulations is fully representative of the simulated cosmological model. Furthermore it is very CPU time-consuming to simulate a large number of different cosmogonies. The exact velocity width distribution will depend on the distribution of virial velocities in a chosen cosmological model weighted by the cross-section for damped absorption,

$$p(\Delta v, N_{\text{HI}} > N_{\text{damp}}, v_{\text{vir}}) = p(\Delta v | N_{\text{HI}} > N_{\text{damp}}, v_{\text{vir}}) \times p(N_{\text{HI}} > N_{\text{damp}} | v_{\text{vir}}) \times p(v_{\text{vir}}). \quad (8)$$

We take the following approach to calculate the distribution of absolute velocity widths. The third factor in equation (8) the relative number of halos with different virial velocities is calculated using the Press-Schechter formalism (Press & Schechter 1974). The cross section for damped absorption is assumed to scale linearly with mass,  $p(N_{\text{HI}} > N_{\text{damp}} | v_{\text{vir}}) \propto M \propto v_{\text{vir}}^3$ . This is the simplest possible scaling suggested by the constant column density threshold defining a DLAS. A good estimate for the first factor is obtainable from our numerical simulations. We found that  $p(\Delta v | N_{\text{HI}} > N_{\text{damp}}, v_{\text{vir}})$  depends mainly on the ratio of  $\Delta v/v_{\text{vir}}$  and only weakly on the virial velocity of the dark matter halo itself. We therefore used the velocity width distribution of all 640 DLAS shown in Fig. 10a. The distribution of absolute velocity widths is obtained by integrating

over virial velocity,

$$p(\Delta v, N_{\text{HI}} > N_{\text{damp}}) = \int_{v_{\text{min}}}^{\infty} p(\Delta v, N_{\text{HI}} > N_{\text{damp}}, v_{\text{vir}}) dv_{\text{vir}}. \quad (9)$$

The result is shown in Fig. 10b for a standard CDM model at  $z = 2.1$  with three different values of  $\sigma_8$  and a minimum virial velocity of  $30 \text{ km s}^{-1}$ . Even the largest observed velocity width,  $\sim 200 \text{ km s}^{-1}$ , can be accommodated in a CDM model with  $\sigma_8$  as low as 0.5 to 0.6. Most of the currently favored variants of hierarchical galaxy formation should therefore have no serious problems in account for the observed velocity width distribution. Constraints on different hierarchical scenarios by the overall incidence rate for damped absorption have been discussed extensively by other authors (see also section 6).

## 6. Damped Ly $\alpha$ absorber — Large disks or protogalactic clumps?

Current hydrodynamical simulations, including those presented here, are undoubtedly unable to model all the details of the spatial distribution and kinematics of the gas in the innermost regions of collapsed dark matter halos. We believe, however, that our simulations already catch many of the significant features and as discussed above they should underestimate rather than overestimate the amount of structure in the density and velocity field. The simulations therefore clearly cast serious doubt on the claim that only objects as massive as present-day spirals can produce the velocity widths of the observed LIS profiles, and that rotation is the only possible interpretation for the shape of the profiles.

Hierarchical structure formation models can explain many other features of the cosmic matter distribution seen in absorption, e.g., the rate of incidence, column density distribution, Doppler parameters, ionization state, sizes, and the opacity of Lyman  $\alpha$  forest clouds, and the abundance, kinematics, temperatures, and ionization conditions of heavy element absorbers (Cen et al. 1994; Hernquist et al. 1996; Petitjean, Mückel & Kates 1995; Miralda-Escudé et al. 1996; Zhang et al. 1997; Croft et al. 1997; Rauch et al. 1997, Bi & Davidsen 1997; Hellsten et al. 1997; paper I&II). The fact that the same models can account for the essential features of DLAS (Katz et al. 1996; Gardner et al. 1997a/b; paper I&II) makes absorption by protogalactic clumps an even more attractive explanation for DLAS. However, some of the observed properties of absorption systems are not unique to hierarchical models and we do not consider the rapidly rotating, large disk hypothesis to be ruled out by our results. Here we briefly comment on other arguments which have been put forward in discussing the nature of DLAS, mostly in favor of DLAS as large, protogalactic disks:

(1) The high column densities:

Large HI column densities of DLAS are indeed reminiscent of present-day disks (e.g. Wolfe 1988). However, simple analytical estimates and the various simulations quoted above show that

these column densities can equally well be produced in gas-rich protogalactic clumps with masses expected in typical hierarchical structure formation models.

(2) The large impact parameter:

Large separations between the absorber and detected emission attributed to associated starlight are taken as indicative of extended, massive objects. However, very few examples are currently known (Møller & Warren 1995; Warren & Møller 1995, Djorgovski 1996). It is not yet clear whether the inferred sizes actually contradict the predictions by hierarchical structure formation scenarios (Mo, Mao & White 1997). This will depend crucially on the detailed gas distribution in the outskirts of protogalactic clumps. Moreover, there are several uncertainties. We do not know yet how emission and absorption properties are related. As demonstrated in section 2 and papers I&II the region responsible for DLAS often contains several protogalactic clumps within a few tens of kpc. Also, the few DLAS identified in emission may only be the tip of the iceberg, at the upper end of the mass and size distribution.

(3) The continuity of  $\Omega_b$ :

$\Omega_b$  in the HI phase of high-redshift DLAS is roughly similar to the baryon content in the stellar component of present-day spirals (Wolfe 1986; Lanzetta et al. 1995; Storrie-Lombardi 1996). This has been interpreted as continuity in baryon content between DLAS and present-day galaxies. If correct this continuity may mean that the gas constituting the stars observed today has already cooled and settled into collapsed objects at these redshifts. The coincidence contains, however, no information on the size distribution of the collapsed objects. Hierarchical models have been shown to reproduce the observed  $\Omega_b$  in DLAS and its evolution with redshift (Kauffmann & Charlot 1994; Ma & Bertschinger 1994; Mo & Miralda-Escudé 1994; Klypin et al. 1995; Gardner et al. 1997a/b; Ma et al. 1997).

(4) The high rate of incidence:

The rate of incidence only depends on the product of space density of the absorbers times their cross section for damped absorption. It gives no constraints on the size of individual absorbers. Hierarchical models have also been shown to reproduce the observed rate of incidence of DLAS and its evolution with redshift (Kauffmann 1996; Baugh et al. 1997).

(5) The alignment of the edge of the absorption profile with the redshift of observed emission:

For two of the DLAS where emission has been observed it is possible to determine the relative position of emission and absorption in redshift space (Lu, Sargent & Barlow 1997). In the first case the emission falls on one edge of the LIS absorption profile in absorption while the strongest absorption feature lies on the opposite edge. In the second case the emission redshift lies roughly at the centre of the absorption profile. If the LIS absorption profiles showing the leading-edge signature were solely due to rotation, if, in addition, the center of emission coincided with the center of the disk and if finally there were no optical depth effects, then the emission redshift should indeed occur preferentially at the edge of the LIS absorption profile opposite to the edge

coinciding with the strongest absorption feature. The situation is, however, similar if the leading edges are due to merging/collision of PGCs. The emission of a stellar continuum would most likely originate in one of the central regions of the merging clumps and should therefore also coincide with one of the two edges of the absorption profile. However, we see no reason why that should happen preferentially opposite to the edge with the strongest absorption feature. Thus, a large number of cases like that reported by Lu et al. would indeed argue for rotation dominating the dynamics.

For completeness, we mention a counterargument against massive disks that has received some attention in the past, the issue of the metallicities in DLAS. The metal abundances ( $[\text{Fe}/\text{H}]$ ) in DLAS at high  $z$  are much lower than expected for local spiral disks (Pettini et al. 1994; Lanzetta, Wolfe, and Turnshek (1995); Lu et al. (1996); Prochaska & Wolfe 1996), which has led to suggestions that DLAS show abundance patterns of dwarf galaxies or galactic halos. In the CDM picture, this inference is correct.

## 7. Conclusions

We have used hydrodynamical simulations of galaxy formation in a cosmological context to study the line profiles of low ionization species associated with damped Ly $\alpha$  absorption systems. Observed velocity widths and asymmetries of the line profiles of the low ionization species are well reproduced by a mixture of rotation, random motions, infall and merging of protogalactic clumps. The asymmetries are mainly caused by random sampling of irregular density and velocity fields of individual halos and by intrinsically asymmetric configurations arising when two or more clumps collide. We show why leading-edge asymmetries occur naturally in the latter case; the dense central regions of the clumps move faster than surrounding less dense material.

We have further shown that the presence of non-circular motions reduces the depth of the potential well necessary to produce a given velocity width compared to a model where the absorption is solely due to rotation. The reduction is typically a factor about 2. The observed velocity width can therefore be explained by gas moving into and within (forming) dark matter halos with typical virial velocities of about  $100 \text{ km s}^{-1}$ . Velocity width and virial velocity are linearly correlated but the scatter is large; there are outliers with large velocity width due to an occasional alignment of clumps with well separated dark matter halos.

Our final conclusion is that asymmetric profiles of the kind observed are not necessarily the signature of rotation and that there is no problem of accommodating the observed velocity widths within standard hierarchical cosmogonies.

## 8. Acknowledgments

We thank Simon White for a careful reading of the manuscript, and Limin Lu, Hojun Mo, Jason Prochaska, and Art Wolfe for very helpful discussions. MR is grateful to NASA for support through grant HF-01075.01-94A from the Space Telescope Science Institute, which is operated by the Association of Universities for Research in Astronomy, Inc., under NASA contract NAS5-26555. Support by NATO grant CRG 950752 and the “Sonderforschungsbereich 375-95 für Astro-Teilchenphysik der Deutschen Forschungsgemeinschaft” is also gratefully acknowledged.

## REFERENCES

- Baugh, C. M., Cole, S., Frenk, C. S., & Lacey, C.G. 1997, ApJ, submitted, astro-ph/9703111
- Bi, H. G., & Davidsen, A.F. 1997, ApJ, 479, 523
- Cen, R., Miralda-Escudé, J., Ostriker, J. P., & Rauch, M. 1994, ApJ, 437, L9
- Djorgovski, S. G., Pahre, M. A., Bechtold, J., & Elston, R. 1996, Nature, 382, 234
- Ferland, G. J. 1993, University of Kentucky Department of Physics and Astronomy Internal Report
- Gardner, J. P., Katz, N., Weinberg, D. H., & Hernquist, L. 1997a, ApJ, in press
- Gardner, J. P., Katz, N., Weinberg, D. H., & Hernquist, L. 1997b, ApJ, in press
- Haehnelt, M.G., Steinmetz, M., & Rauch, M. 1996, ApJ, 465, L95 (paper I)
- Haardt, F., & Madau, P. 1996, ApJ, 461, 20
- Hellsten, U., Davé, R., Hernquist, L., Weinberg, D. H., & Katz, N. 1997, ApJ, in press
- Hernquist, L., Katz, N., Weinberg, D. H., & Miralda-Escudé, J. 1996, ApJ, 457, L5
- Kauffmann, G. A. M. 1996, MNRAS, 281, 475
- Katz, N., Weinberg, D. H., Hernquist, L., & Miralda-Escudé J. 1996, ApJ, 457, L57
- Klypin, A., Borgani, S., Holtzman, J., & Primack, J. 1995, ApJ, 44, 1
- Lanzetta, K. M., Wolfe, A. M., Turnshek, D. A., Lu, L., McMahon, R. G., & Hazard, C. 1991, ApJS, 77, 1
- Lanzetta, K. M., Wolfe, A. M., & Turnshek, D. A. 1995, ApJ, 440, 435
- Lu, L., Sargent, W. L. W., & Barlow, T. A. 1997, ApJ, in press, astro-ph/9701116
- Lu, L., Sargent, W. L. W., Barlow, T. A., Churchill, C. W., & Vogt, S. 1996, ApJS, 107, 475
- Ma, C.-P., & Bertschinger E. 1994, ApJ, 434, L5
- Miralda-Escudé, J., Cen, R., Ostriker, J.P., & Rauch, M. 1996, ApJ, 471, 582
- Mo, H. J. 1994, MNRAS, 269, 49
- Mo, H. J., & Miralda-Escudé, J. 1994, ApJ, 430, L25
- Mo, H. J., & Miralda-Escudé, J. 1996, ApJ, 469, 589

- Mo, H. J., Mao, S., & White, S. D. M., 1997, in preparation
- Møller, P., & Warren, S. J. 1995, in *Galaxies in the Young Universe*, eds. Hippelein, Meisenheimer & Röser, p88
- Navarro, J. F., & Steinmetz, M. 1997, *ApJ*, 478, 13
- Pettini, M., Smith, L. J., Hunstead, R. W., & King, D. L. 1994, *ApJ*, 426, 79
- Press, W. H., & Schechter, P. L. 1974, *ApJ*, 187, 425
- Prochaska, J. X., & Wolfe, A. M. 1996, *ApJ*, 470, 403
- Prochaska, J. X., & Wolfe, A. M. 1997, *ApJ*, in press, astro-ph/9704169
- Rauch, M., Haehnelt, M.G., & Steinmetz, M. 1997, *ApJ*, 481, 601 (paper II)
- Steinmetz, M. 1996, *MNRAS*, 278, 1005
- Storrie-Lombardi, L. J., McMahon, R. G., & Irwin, M. J. 1996, *MNRAS*, 283, L79
- Viegas, S. M. 1995, *MNRAS*, 276, 268
- Warren, S. J., & Møller, P. 1995, in *New Light on Galaxy Evolution*, IAU Symposium 171, Heidelberg June 1995, in press
- Wolfe, A. M., Turnshek, D. A., Smith, H. E., & Cohen, R. D. 1986, *ApJ*, 61, 249
- Wolfe, A. M. 1988, in *QSO Absorption Lines: Probing the Universe*, Proc. of the QSO Absorption Line Meeting, Baltimore, 1987, Cambridge University Press
- Wolfe, A. M. 1995, in *QSO Absorption Lines*, Proc. ESO Workshop, ed. G.Meylan (Heidelberg: Springer), p. 13.
- Wolfe, A. M., Lanzetta, K. M., Foltz, C. B., & Chaffee, F. H. 1995, *ApJ*, 454, 698